

Analysis of a Numerical Scheme for Bioheat Simulations of Cryosurgery and its Experimental Validation on a Phantom Material

Michael R. Rossi and Yoed Rabin*
Biothermal Technology Laboratory
Department of Mechanical Engineering
Carnegie Mellon University
Pittsburgh, PA, USA

Abstract - *As part of an ongoing effort to develop computerized planning tools for cryosurgery, the current study focuses on validating a numerical technique for bioheat transfer simulations. The long-term goal is to develop a planning tool for cryosurgery that takes a 3D reconstruction of a target region, and suggests the best cryoprobe layout. To make the planning tool clinically relevant, a new finite difference numerical technique has been developed that allows for short (clinically relevant) runtime of cryosurgical simulations. The objectives of the current study are to perform a 2D experimental validation of the technique, and to determine an optimal grid discretization for a given experimental system.*

Keywords: Cryosurgery, Computerized Planning, Bioheat Transfer, Simulation, Experimental Validation

1 Introduction

Cryosurgery is the destruction of undesired biological tissues by freezing [1]. Modern cryosurgery is frequently performed as a minimally-invasive procedure, in which a number of cryoprobes (up to about a dozen) are inserted into the target area to be treated [2]. While there is an extensive body of literature on the factors affecting the success of cryosurgery (with the lethal temperature threshold of -45°C as possibly the most universally accepted factor in recent years [3]), it is the match between the frozen region contour and the outer surface of the target region which is currently used for cryosurgery control. This match is evaluated with the application of an imaging device, such as ultrasound or MRI [4-7]. The cryoprobe layout is a key factor for achieving the highest quality of that match and, therefore, for the success of the cryosurgery.

To date, cryoprobe localization is an art held by the cryosurgeon, based on the surgeon's own experience and accepted practices. Suboptimal cryoprobe localization may leave areas in the target region untreated, may lead to cryoinjury of healthy surrounding tissues, require an

unnecessarily large number of cryoprobes, increase the duration of the surgical procedure, and may increase the likelihood of post cryosurgery complications, all of which affect the quality and cost of the medical treatment. Computerized planning tools would help to alleviate these difficulties, which is the subject matter of this ongoing research program at the Biothermal Technology Laboratory [8-14].

Recently, a new 3D finite difference numerical scheme was presented, which has been developed for short runtime of cryosurgery simulations [12], in order to make several prototypes of computerized planning tools clinically relevant [8-10,13]. The current study is focused on experimental validation of the numerical scheme, using liquid nitrogen-based cryoprobes and a urethral warmer prototype. More specifically, a case study is presented--based on a 2D experimental result--aimed at determining the best design of the finite difference grid for the specific experimental system. This study also includes imaging analysis tools to reconstruct the resulting frozen region from video recordings.

2 Experimental Setup and Analysis

The experimental setup is designed for 2D cryosurgery simulation in a gelatin solution as a phantom material, where the 2D setup is representative of a prostate cross-section. The experimental setup has been developed recently [15], and is presented here in brief, for the completeness of presentation. The thermophysical properties of pure water are much like those of soft tissues [9,11]; gelatin is added to prevent convective heat transfer in the domain. In order to accentuate the contrast between the frozen and unfrozen regions in the gelatin, blue food dye is added to the gelatin solution.

A proprietary cryodevice is used in the current study, which is a modification of an earlier device, based on liquid-nitrogen cooling [16,17], and similar to the original cryoprobes invented by Cooper and Lee in 1961 [1]. The new cryoprobes are made of copper, with an external

* Corresponding author: rabin@cmu.edu

diameter of 3.2 mm. Up to six probes can be used concurrently, with a cooling rate of about 33°C/min in the first three minutes of operation, and a minimum operation temperature of about -110°C.

Urethral warming in the current setup is simulated with a cryoheater [11,18]. It is placed inside a 7 mm OD thin-wall brass tube, and a temperature controller is used to maintain the temperature of the cryoheater at a constant 25°C throughout the experiment. The heater, along with the cryoprobes, are inserted through holes in a gelatin container made of 5 mm-thick Plexiglas plates, with a gelatin chamber of 25 mm × 200 mm × 200 mm.

For the current study, an experiment was performed and video recorded, using six cryoprobes. Figure 1(a) shows the original experimental image used for this study, captured at eight minutes into the recorded video. Reconstruction of the frozen region from this image is performed in two stages: registration and segmentation. Registration is done manually by identifying the exact pixel locations of each cryoprobe and the cryoheater (pixel diameter is 0.28 mm).

To prepare the image for segmentation, the contrast is enhanced and the image is converted from true color RGB to grayscale. Next, in order to sharpen the edge between the frozen region and the surrounding domain, the MATLAB filter “unsharp” is used, and the result is shown

in Fig. 1(b). Because of the high contrast level achieved, a simple region-growing segmentation technique, similar to methods used in [19,20], can be applied.

The segmentation of the experimental frozen region begins from seed points located at the center of the cryoprobe locations, and surrounding pixels are added to the domain based on their level of intensity and proximity to previously added pixels. This process is repeated until no additional pixels can be identified as representative of the frozen region. Following the completion of the region growing segmentation, a dilation transformation [21] is performed to finalize the reconstruction. Dilation enlarges the segmented image by adding pixels to its boundary, in order to fill small holes and gaps. Figure 1(c) displays the result for the image displayed in Fig. 1(b) upon completion of the segmentation and dilation.

3 Numerical Simulations

For computerized planning, it is assumed that in previous studies [8,10,12,22] the classic bioheat equation [23] can be used to model heat transfer during cryosurgery of the prostate:

$$C \frac{\partial T}{\partial t} = \nabla \cdot (k \nabla T) + \dot{w}_b C_b (T_b - T) + q_{met} \quad (1)$$

where C is the volumetric specific heat of the tissue, T is

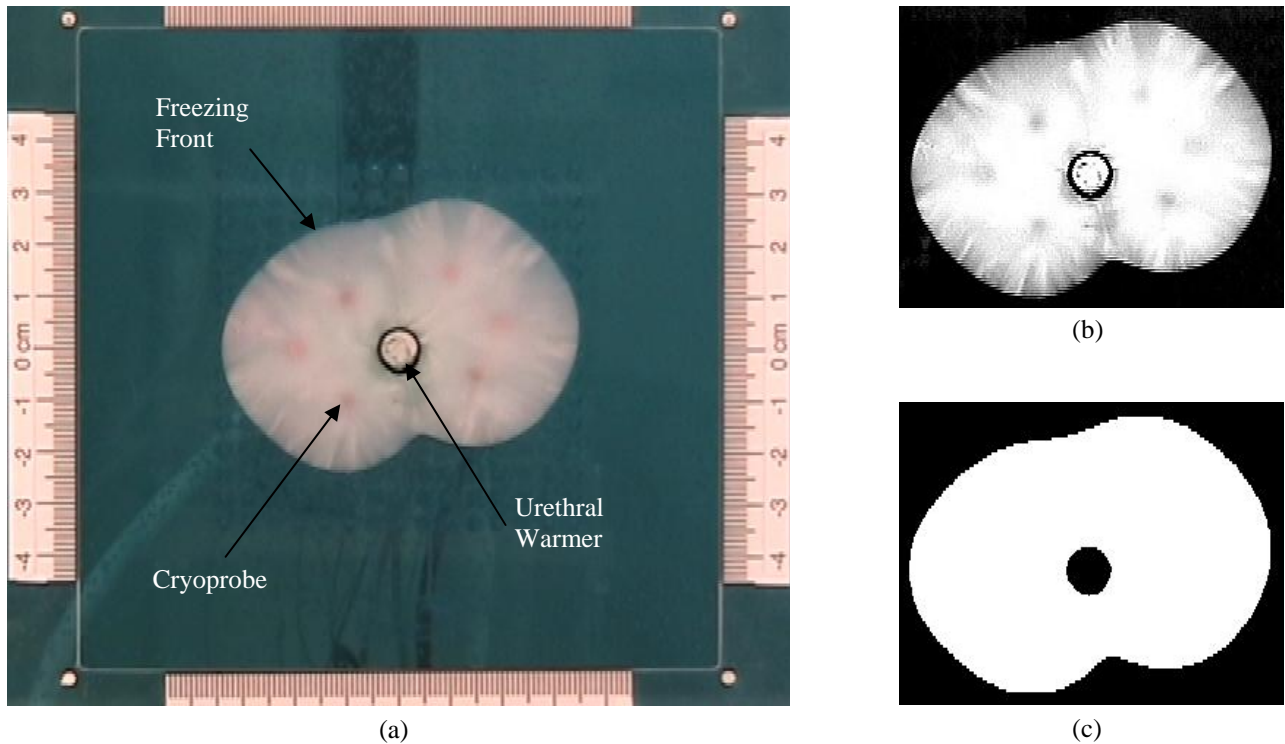


Figure 1: Segmentation of the experimental image: (a) Experimental bitmap image captured from the video; (b) The frozen region after maximizing contrast; (c) Segmented frozen region, where the white portion represents the result to be compared with the numerical simulation.

the temperature, t is the time, k is the thermal conductivity of the tissue, \dot{w} is the blood perfusion volumetric flow rate per unit volume of tissue, C_b is the volumetric specific heat of the blood, T_b is the blood temperature entering the thermally treated area, and q_{met} is the metabolic heat generation.

A numerical technique has been presented to solve Eq. (1), using a finite difference scheme [22]. More recently, that scheme has been optimized for short runtime [12], using a variable grid technique, in order to make its runtime clinically relevant for computerized planning of cryosurgery [10]. Figure 2 schematically illustrates a representative 2D domain, along with the superimposed experimental frozen region contour. Notice that a fine grid is used in regions of steep temperature gradients (near cryoprobes) and complex contours (around the urethral warmer). For the current study, the cryoprobes are modeled so that they include all of the nodes within 1.4 mm from their center. Thus, the cryoprobe shape in the current study is dependent on the grid size. Similarly, the urethral warmer includes all of the nodes within 3.6 mm of its center location (held at a temperature of 25°C for the duration of the simulation). To ensure that the centers of all cryoprobes and the urethral warmer lie on simulated grid nodes, the fine grid size used must be equal to the experimental grid spacing (5 mm) divided by an integer. A standard domain area was applied to all numerical simulations having dimensions of 130 mm \times 130 mm.

In addition to lowering the number of simulation nodes, the use of variable grid sizes allows for the application of longer time intervals for larger grid sizes, due to stability criteria [22]. Thus, simulated run time for variable grid solutions can be further shortened if the thermal history at any given point progresses in accordance with its own

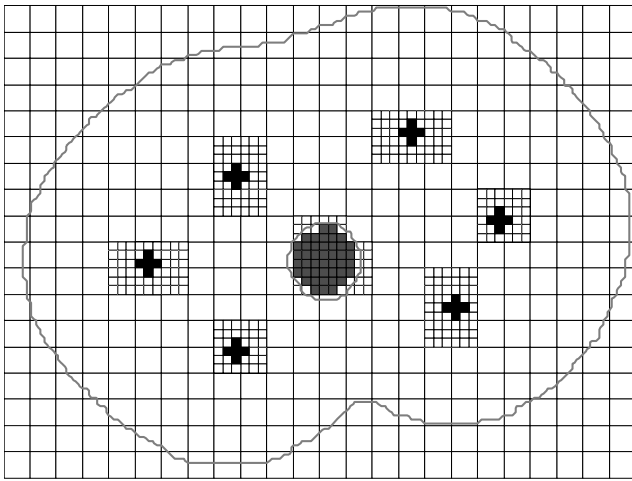


Figure 2: Schematic illustration of the simulation grid used for Test #17, along with the superimposed experimental freezing front; the fine and coarse grid sizes for this variable grid case are set to 1 mm and 3 mm, respectively.

unique time interval, associated with local stability criteria.

The current study is performed using a 1.6% gelatin solution, where the physical properties of the pure water are well documented to a high degree of certainty. Since this comparison is not performed on a biological tissue, the blood perfusion term and metabolic heat generation are set to zero. While water--as a pure material--freezes at a unique temperature, biological tissues freeze over a wide temperature range, and the numerical technique has been developed accordingly. The numerical technique is based on the enthalpy approach, with an effective specific heat which incorporates the latent heat. For the current study, a phase transition temperature range of -2°C to +2°C is assumed for pure water.

4 Method for Comparison

Comparison between experimental data and numerical results in the current study is based on the evolution of the frozen region area and shape. For this purpose, and consistent with prior work [8-10,12], a defect is defined as a difference in frozen region area between experimental and simulated results. The value for the total defect is calculated using:

$$D_T = \frac{1}{A_E} \int_{A_s} w dA_s \cong \sum_m w_m A_m \quad (2)$$

where A_E is the area of the reconstructed experimental frozen region, A_s is the total area of the simulated domain, m is an index representing all grid points in the simulated domain, and w is a weight function:

$$w_m = \begin{cases} 1 & -2^\circ\text{C} < T_m & \text{interior to exp. frozen reg.} \\ 0 & T_m \leq -2^\circ\text{C} & \text{interior to exp. frozen reg.} \\ 1 & T_m \leq -2^\circ\text{C} & \text{exterior to exp. frozen reg.} \\ 0 & -2^\circ\text{C} < T_m & \text{exterior to exp. frozen reg.} \end{cases} \quad (3)$$

where T_m is the simulated temperature at grid point m . The temperature isotherm of -2°C was selected to represent the freezing front for the numerical simulation, since it is the lower boundary of the phase transition range and corresponds to the complete release of latent heat.

In order to compare the simulated frozen region contour with the experimental data, the results of the numerical simulations are interpolated into the image pixel grid, using a bilinear interpolation, for the evaluation of Eq. (2) and the graphical presentation of temperature isotherms with experimental results.

For simplicity, the temperatures of all the cryoprobes are set to the minimum value (-110 °C) for the entirety of the numerical simulations. This assumption leads to inaccuracy

Table 1: Results of 2D cryosurgical simulations with six cryoprobes at the time of minimum defect with respect to experimental data, where GS_F and GS_C are the grid sizes for the fine and coarse grids, respectively, N_P is the number of nodes used for modeling a cryoprobe, A_P and P_P are the area and perimeter of the simulated cryoprobes, respectively, N_F and N_C are the overall numbers of fine and coarse grid nodes, respectively, T_S is the simulation time when minimum defect is reached, D_T is the total defect, A_S is the simulated frozen region area, ΔS is the average difference in freezing front location between the numerical solution and experimental data, and T_R is the runtime for the simulation; the area of the experimental target region is 2652 mm².

| Test # | GS_F , mm | GS_C , mm | N_P | A_P , mm ² | P_P , mm | N_F | N_C | T_S , sec | D_T , % | A_S , mm ² | ΔS , mm | T_R , sec |
|--------|-------------|-------------|-------|-------------------------|------------|-------|-------|-------------|-----------|-------------------------|-----------------|-------------|
| 1 | 0.50 | 0.50 | 21 | 5.3 | 10.0 | 0 | 66955 | 325 | 1.1 | 2660 | 0.14 | 518 |
| 2 | 0.63 | 0.63 | 13 | 5.1 | 12.5 | 0 | 42771 | 325 | 1.2 | 2665 | 0.15 | 211 |
| 3 | 0.83 | 0.83 | 9 | 6.3 | 10.0 | 0 | 23971 | 317 | 1.5 | 2642 | 0.19 | 54.5 |
| 4 | 1.00 | 1.00 | 5 | 5.0 | 12.0 | 0 | 16611 | 337 | 2.1 | 2650 | 0.27 | 33.6 |
| 5 | 1.25 | 1.25 | 5 | 7.8 | 15.0 | 0 | 10579 | 302 | 1.7 | 2635 | 0.21 | 12.8 |
| 6 | 1.67 | 1.67 | 1 | 2.8 | 6.7 | 0 | 6078 | 429 | 2.1 | 2642 | 0.27 | 5.3 |
| 7 | 2.50 | 2.50 | 1 | 6.3 | 10.0 | 0 | 2595 | 374 | 2.9 | 2625 | 0.37 | 1.5 |
| 8 | 0.50 | 1.00 | 21 | 5.3 | 10.0 | 542 | 16733 | 331 | 1.4 | 2650 | 0.18 | 33.5 |
| 9 | 0.50 | 1.50 | 21 | 5.3 | 10.0 | 720 | 7302 | 339 | 1.8 | 2654 | 0.22 | 16.5 |
| 10 | 0.50 | 2.00 | 21 | 5.3 | 10.0 | 786 | 4168 | 352 | 2.0 | 2657 | 0.25 | 14.1 |
| 11 | 0.63 | 1.25 | 13 | 5.1 | 12.5 | 462 | 10474 | 333 | 1.6 | 2662 | 0.20 | 15.4 |
| 12 | 0.63 | 1.88 | 13 | 5.1 | 12.5 | 579 | 4688 | 339 | 2.0 | 2647 | 0.25 | 8.8 |
| 13 | 0.63 | 2.50 | 13 | 5.1 | 12.5 | 786 | 2650 | 347 | 2.8 | 2641 | 0.35 | 10.0 |
| 14 | 0.83 | 1.67 | 9 | 6.3 | 10.0 | 310 | 5838 | 329 | 2.1 | 2635 | 0.27 | 5.5 |
| 15 | 0.83 | 2.50 | 9 | 6.3 | 10.0 | 477 | 2542 | 340 | 3.0 | 2639 | 0.39 | 3.8 |
| 16 | 1.00 | 2.00 | 5 | 5.0 | 12.0 | 294 | 4144 | 337 | 2.9 | 2600 | 0.37 | 3.5 |
| 17 | 1.00 | 3.00 | 5 | 5.0 | 12.0 | 366 | 1805 | 359 | 3.7 | 2617 | 0.47 | 2.7 |
| 18 | 1.25 | 2.50 | 5 | 7.8 | 15.0 | 254 | 2633 | 322 | 2.9 | 2664 | 0.37 | 2.0 |
| 19 | 1.25 | 3.75 | 5 | 7.8 | 15.0 | 321 | 1117 | 329 | 4.2 | 2613 | 0.54 | 1.8 |
| 20 | 1.67 | 3.33 | 1 | 2.8 | 6.7 | 154 | 1404 | 455 | 4.1 | 2640 | 0.52 | 1.4 |
| 21 | 2.50 | 5.00 | 1 | 6.3 | 10.0 | 138 | 640 | 400 | 5.6 | 2628 | 0.72 | 1.0 |

in the predicted simulation time; however, the main goal associated with the numerical simulations is not to predict run time, but rather to best match the target region associated with computerized planning [12]. Thus, each simulation is run until a minimum defect is found.

In addition to the defect comparison, the average difference in freezing front location, ΔS , is determined in order to gain more insight about the magnitude of the mismatch. This value is calculated by dividing the absolute defect area by the perimeter of the experimental frozen region.

5 Results and Discussion

A total of 21 numerical simulations were performed in the current study, each with a different grid discretization. Simulated results were obtained using a

cryosurgery simulator prototype, written in C++, implemented with Visual Studio, and run on a 3.4 GHz Pentium 4 machine, with 1.5 GB of memory and 800 MHz front side bus; the simulator was optimized for runtime. All of the simulations were compared with the experimental data shown in Fig. 1(c), and the results are listed in Table 1.

In the first seven numerical simulations, a uniform grid size was used throughout the domain. These tests were performed in order to observe how the quality of the comparison varies with respect to the grid size and the modeling of the cryoprobes and urethral warmer. With respect to the geometrical modeling of the cross-section of the cryoprobes, a large variation is observed within the first seven tests. The number of nodes used to model a cryoprobe ranges from 1 to 21. In addition, a large

variation is also seen in the area (2.8 mm^2 to 7.8 mm^2) and perimeter (6.7 mm to 15.0 mm) of the cryoprobes. These large discrepancies in cryoprobe size lead to a considerable variation in the simulation duration (302 sec to 429 sec). Nevertheless, even with these large variations in cryoprobe size and discretization, the value for defect does not exceed 2.9% for any of the uniform grid simulations.

The best match of all of the results is obtained with Test #1, which uses a fine 0.5 mm grid size throughout the simulated domain. The value for defect was found to be 1.1%, which equates to an average uncertainty in freezing front location of 0.14 mm. The quality of this agreement is reflected in Fig. 3(a), where both the simulated and segmented experimental freezing fronts are displayed. The results listed in Table 1 for Test #2 (using a 0.625 mm grid) were almost identical to Test #1, implying that the solution has fully converged when a grid size of 0.625 mm or less is used. In general, considering all of the uncertainties associated with the experimental data and numerical modeling, good agreement is found between these fine grid simulations and experiment data.

As the grid size increases, the quality of agreement between numerical results and experimental data decreases.

For the 2.5 mm grid used in Test #7, a small but noticeable disagreement is observed between simulation results and the experiment data, Fig. 3(b). The majority of the disagreement is prevalent around the urethral warmer, which is a result of the poor modeling of the warmer due to the large (2.5 mm) grid size (the warmer was simply modeled as a 3×3 square). Around the outer perimeter of the freezing front, the agreement is still good, even with the relatively large grid size and simplistic modeling of the cryoprobes and urethral warmer; this is the least satisfactory result of the uniform grid solutions, which suggests that the quality of the simulated results is adequate.

Based on the quality and consistency of the uniform grid simulation results, it can be concluded that precise modeling of the cryoprobes is not essential for obtaining an accurate prediction of the final freezing front shape and size for cryosurgical applications. A wide range of cryoprobe sizes and discretizations provided similar simulation results. Even the two cases with the largest discrepancy in cryoprobe size (Tests #5 and #6), provided almost identical final simulated results, with respect to defect, simulated frozen region area, and average freezing front difference. This result is very important, as it

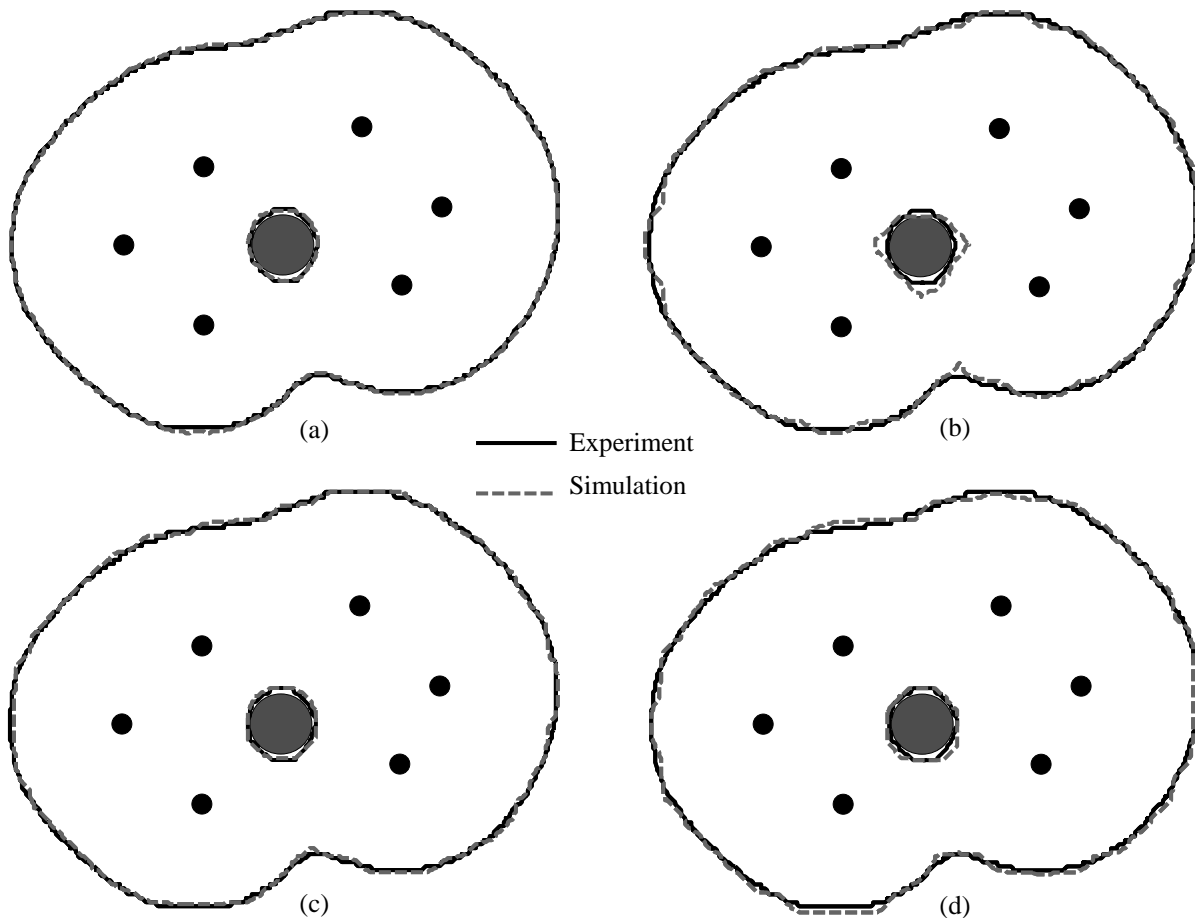


Figure 3: Comparison between experimental and simulated freezing fronts for four different simulation cases: (a) Test #1; (b) Test #7; (c) Test #12; (d) Test #18.

demonstrates the ability to use larger grid sizes, while maintaining high certainty in the simulated results. By replacing the grid structure of Test #1 with that of Test #6, runtime is decreased by two orders of magnitude.

The discussion now turns to the variable grid size simulation results. For Tests #8, #9, and #10, small to large grid ratios of 1:2, 1:3, and 1:4 were used, respectively, with a 0.5 mm fine grid size. Compared to the uniform 0.5 mm grid solution, these variable grid cases reduced runtime by over an order of magnitude, with minimal increase in error. The simulation result with a grid ratio of 1:3 (Test #9) appears to yield the best results in that group. It is twice as fast as the 1:2 grid ratio case, with comparable accuracy, and more accurate than the 1:4 grid ratio case, with comparable runtime. These same trends are seen for Tests #11 through #13, where a 0.625 mm fine grid size was used. In Fig. 3(c), the simulated result for Test #12 is compared to the experimental data (run time for the simulation was 8.8 sec.)

As one would expect, runtime decreases with increased grid size, while the agreement with experimental data becomes weaker. For Test #14, runtime of 5.5 sec and defect of 2.1% are observed. For Test #16, the runtime decreases to 3.5 sec, but the defect increases to 2.9%. Finally, for Test #18, an optimal balance between accuracy and speed is found. Test #18 uses a 1.25 mm fine grid size, with a 1:2 grid ratio. The percent defect is 2.9%, corresponding to an average freezing front uncertainty of 0.37 mm, Fig. 3(d). Although the agreement is not as good as with Tests #1 and #12, the quality is still adequate for cryosurgical simulations, and the runtime is only 2.0 seconds. Compared with Test #7 (which has similar defect and runtime values), the simulation results of Test #18 indicate more accurate modeling of the heat transfer around the urethral warmer.

6 Summary and Conclusions

The current study focuses on experimental validation of a variable-grid numerical scheme for computerized planning of cryosurgery. A total of 21 numerical simulations were performed in this study, and compared to experimental data. Results indicate that, within the range of the numerical grid parameters tested, precise modeling of the cryoprobes is not warranted for cryosurgical simulation, provided that simulations are run until minimum defect is reached. In addition, for the given experimental design, an optimal grid discretization, based on accuracy and runtime, was determined for the numerical scheme, using a 1.25 mm fine grid size along with a grid ratio of 1:2. The percent defect associated with this discretization was found to be 2.9%, corresponding to an average freezing front uncertainty of 0.37 mm. In the context of prostate cryosurgery, where uncertainties with respect ultrasound imaging can easily exceed 1 mm, it is

concluded that the given grid discretization is adequate for the purpose of computerized planning.

7 Acknowledgement

This project is supported by the National Institute of Biomedical Imaging and Bioengineering (NIBIB) – NIH, grant # R01-EB003563-01,02,03,04.

8 References

- [1] I.S. Cooper and A. Lee, Cryostatic congelation: a system for producing a limited controlled region of cooling or freezing of biological tissues, *J. Nerve Mental Dis.*, Vol. 133, pp. 259-263, 1961.
- [2] A.A. Gage, Cryosurgery in the treatment of cancer, *Surg. Gynecol. Obstet.*, Vol. 174, pp. 73-92, 1992.
- [3] A.A. Gage and J. Baust, Mechanisms of tissue injury in cryosurgery, *Cryobiology*, Vol. 37, pp. 171-186, 1998.
- [4] G.M. Onik, J.K. Cohen, G.D. Reyes, B. Rubinsky, Z.H. Chang, and J. Baust, Transrectal ultrasound-guided percutaneous radical cryosurgical ablation of the prostate, *Cancer*, Vol. 72(4), pp. 1291-1299, 1993.
- [5] G.M. Onik, J.C. Gilbert, W. Hoddick, R. Filly, P. Callen, B. Rubinsky, and L. Farrel, Sonographic monitoring of hepatic cryosurgery in an experimental animal model, *Am. J. of Roentgenol.*, Vol. 144(5), pp. 1043-1047, 1985.
- [6] B. Rubinsky, J.C. Gilbert, G.M. Onik, M.S. Roos, S.T.S. Wong, and K.M. Brennan, Monitoring cryosurgery in the brain and the prostate with proton NMR, *Cryobiology*, Vol. 30, pp. 191-199, 1993.
- [7] T. Schulz, S. Puccini, J.P. Schneider, and T. Kahn, Interventional and intraoperative MR: review and update of techniques and clinical experience, *Eur. Radiol.*, Vol. 14(12), pp. 2212-2227, 2004.
- [8] D.C. Lung, T.F. Stahovich, and Y. Rabin, Computerized planning for multiprobe cryosurgery using a force-field analogy, *Computer Methods in Biomechanics and Biomedical Engineering*, Vol. 7(2), pp. 101-110, 2004.
- [9] Y. Rabin, D.C. Lung, and T.F. Stahovich, Computerized planning of cryosurgery using cryoprobes and cryoheaters, *Technology in Cancer Research and Treatment*, Vol. 3(3), pp. 227-243, 2004.
- [10] D. Tanaka, K. Shimada, and Y. Rabin, Two-phase Computerized Planning of Cryosurgery Using Bubble-packing and Force-field Analogy, *ASME Journal of Biomechanical Engineering*, Vol. 128(1), pp. 49-58, 2006.

[11] Y. Rabin and T.F. Stahovich, Cryoheater as a means of cryosurgery control, *Physics in Medicine and Biology*, Vol. 48, pp. 619-632, 2003.

[12] M.R. Rossi, D. Tanaka, K. Shimada, and Y. Rabin, An efficient numerical technique for bioheat simulations and its application to computerized cryosurgery planning, *Computer Methods and Programs in Biomedicine*, Vol. 85(1), pp. 41-50, 2007.

[13] D. Tanaka, M.R. Rossi, K. Shimada, and Y. Rabin, Towards intra-operative computerized planning of prostate cryosurgery, *The International Journal of Medical Robotics and Computer Assisted Surgery*, 2007, in press.

[14] Biothermal Technology Laboratory at Carnegie Mellon University, Developing computerized tools for cryosurgery planning:
<http://www.me.cmu.edu/faculty1/rabin/RabinCryoPlan.htm>

[15] M.R. Rossi and Y. Rabin, Experimental verification of numerical simulations of cryosurgery with application to computerized planning, 2007, submitted.

[16] Y. Rabin, T.B. Julian, and N. Wolmark, A compact cryosurgical apparatus for minimal-invasive cryosurgery, *Biomedical Instrumentation & Technology*, Vol. 31, pp. 251-258, 1997.

[17] Y. Rabin, T.B. Julian, and N. Wolmark, Method and apparatus for minimal-invasive cryosurgery, 2000, US Patent No. 6,039,730.

[18] Y. Rabin, T.B. Julian, and N. Wolmark, Method and apparatus for heating during cryosurgery, 1999, US Patent No. 5,899,897.

[19] Y.L. Chang and X. Li, Adaptive image region-growing, *IEEE Transactions on Image Processing*, Vol. 3(6), pp. 868-872, 1994.

[20] R. Pohle and K. Toennies, Segmentation of medical images using adaptive region growing, In: *Proc. SPIE Medical Imaging*, eds: M. Sonka and K.M. Hanson, Vol. 4322, pp. 1337-1346, 2001.

[21] J. Serra, *Image Analysis and Mathematical Morphology*, Academic Press, London, 1982.

[22] Y. Rabin and A. Shitzer, Numerical solution of the multidimensional freezing problem during cryosurgery, *ASME Journal of Biomechanical Engineering*, Vol. 120(1), pp. 32-37, 1998.

[23] H.H. Pennes, Analysis of tissue and arterial blood temperatures in the resting human forearm, *J. App. Phys.*, Vol. 1, pp. 93-122, 1948.